Special issue article

Institution of MECHANICAL ENGINEERS
Journal of SYSTEMS AND CONTROL ENGINEERING

Proc IMechE Part I:
J Systems and Control Engineering
2018, Vol. 232(6) 695–708

DOI: 10.1177/0959651818755292
journals.sagepub.com/home/pii
SAGE

Fault indicators and unique mode-dependent state equations from a fixed-causality diagnostic bond graph of linear models with ideal switches

Wolfgang Borutzky

Abstract

Analytical redundancy relations are fundamental in model-based fault detection and isolation. Their numerical evaluation yields a residual that may serve as a fault indicator. Considering switching linear time-invariant system models that use *ideal* switches, it is shown that analytical redundancy relations can be systematically deduced from a diagnostic bond graph with *fixed* causalities that hold for all modes of operation. Moreover, as to a faultless system, the presented bond graph–based approach enables to deduce a unique implicit state equation with coefficients that are functions of the discrete switch states. Devices or phenomena with fast state transitions, for example, electronic diodes and transistors, clutches, or hard mechanical stops are often represented by *ideal* switches which give rise to variable causalities. However, in the presented approach, *fixed* causalities are assigned only once to a diagnostic bond graph. That is, causal strokes at switch ports in the diagnostic bond graph reflect only the switch-state configuration in a specific system mode. The actual discrete switch states are implicitly taken into account by the discrete values of the switch moduli. The presented approach starts from a diagnostic bond graph with *fixed* causalities and from a partitioning of the bond graph junction structure and systematically deduces a set of equations that determines the wanted residuals. Elimination steps result in analytical redundancy relations in which the states of the storage elements and the outputs of the ideal switches are unknowns. For the later two unknowns, the approach produces an implicit differential algebraic equations system. For illustration of the general matrix-based approach, an electromechanical system and two small electronic circuits are considered. Their equations are directly derived from a diagnostic bond graph by following causal paths and are reformulated so that they conform with the matrix equations obtained by the formal approach based on a partitioning of the bond graph junction structure. For one of the three mode-switching examples, a fault scenario has been simulated.

Keywords

Fault detection and isolation, mode-switching linear time-invariant models, ideal switches, diagnostic bond graphs, fixed causalities generation of analytical redundancy relations, mode-dependent implicit state space model

Date received: 31 July 2017; accepted: 26 November 2017

Introduction

In the beginning, bond graph (BG) modelling was mainly confined to continuous time models for the purpose of an analysis or a simulation of engineering systems. In the course of the last two decades, the BG methodology was extended to also capture hybrid models.

Strömberg et al.[1] extended the small set of fundamental BG elements by introducing the ideal switch as another basic BG element accepting that computational causalities at least in some parts of a BG become mode-dependent. To compensate for causality changes, Asher[2] introduced so-called causality resistors. Buisson et al. also used ideal switches and presented a matrix-based approach to the generation of an implicit state equation from a BG of a switching linear time-invariant (LTI) model for a reference mode. Equations for any other mode of operation are deduced from the set of equations for the reference mode.[3] Margetts[4] also follows the variable causality approach but uses controlled junctions introduced by Mosterman,[5] marks causalities in the BG that change due to switch state changes by additional dashed causal strokes that indicate the causal

Bonn-Rhein-Sieg University of Applied Sciences, Sankt Augustin, Germany

Corresponding author:
Wolfgang Borutzky, Bonn-Rhein-Sieg University of Applied Sciences, 53754 Sankt Augustin, Germany.
Email: wolfgang.borutzky@h-brs.de

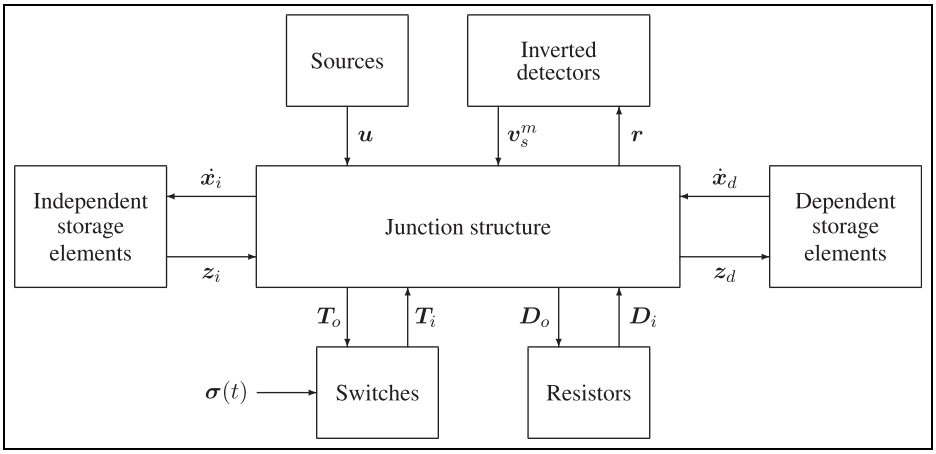

Figure 1. Block diagram of a general bond graph.

configuration after the commutation of some switches and distinguishes between static and dynamic causalities. Other than Buisson et al., she derives a single implicit state equation for all modes of operation.

Ensuing, various publications have demonstrated that BGs can also serve model-based fault detection and isolation (FDI).[6] The main contribution of BGs to model-based FDI is that analytical redundancy relations (ARRs) can be systematically deduced from a diagnostic bond graph (DBG) with detectors in inverted causality and storage elements in derivative causality.[7] The numerical evaluation of ARRs provides fault indicators, and their structure enables to detect possible fault candidates. ARRs are also a possible basis for model-based failure prognosis.[8,9]

The next step during the last years has been to apply BG model-based FDI to hybrid models.[10,11] In Wang et al.,[11] ideal switching is captured by controlled junctions, while the literature[10,12,13] uses non-ideal switches, so that causalities remain fixed, that is, mode-independent.

This article shows that a set of ARRs as well as a set of unique implicit state equations can be deduced from a DBG with *fixed* causalities of a switching LTI system model. The coefficients in both sets of equations are functions of the discrete switch states. Switching devices are taken into account by *ideal* switches. Ideal switches entail variable causality, at least locally. Nevertheless, *fixed* causalities are assigned only once so that a DBG is obtained. As to the causalities at switch ports, the BG reflects only a specific configuration of switch states, that is, a single system mode of operation. From such a DBG with fixed causalities, a unique set of ARRs including discrete switch states is derived. The result is obtained using an *implicit* equation for the commutation of switches and by disregarding the causal strokes switch ports have got by the causality assignment. The ARRs are given implicitly. In order to evaluate them, first, an algebraic or a differential algebraic equations (DAE) system must be solved. This also applies to time continuous models in case non-linear constitutive element equations prevent the elimination of unknowns.

As to continuous time models, Ould Bouamama et al.[14] presented a procedure for the systematic derivation of ARRs from a BG, and a module of the modelling and simulation software environment Symbols[15] supports their generation.[16] To the best knowledge of the author, a systematic generation of a *single* set of ARRs for all modes of operation from a DBG with *fixed* causalities of a *hybrid* model using *ideal* switches hasn't been reported in the literature.

As in Buisson et al.,[3] the general matrix-based equations formulation starts from the well-known block diagram of a general BG extended by a field of ideal switches and a partitioning of the junction structure (JS) matrix. Equations obtained from the partitioning of the JS matrix are reformulated so that the outputs of the JS into the switch field can be inserted into the *implicit* switch equation resulting in an implicit ordinary differential equation (ODE) for the states of the storage elements. The formal approach is illustrated by three small example systems. Each of them is characterized by a particular feature.

Formal matrix-based approach

This article confines to mode-switching LTI models as a subset of general (non-linear) hybrid system models. As in Buisson et al.,[3] the general matrix-based equations formulation starts from the well-known block diagram of a general BG extended by a field of ideal switches and adds a field of inverted detectors (Figure 1). The grouping of elements into fields results in a partitioning of the JS matrix. Equation (1) obtained from the partitioning of the JS matrix is reformulated so that the outputs of the JS into the switch field can be inserted into an *implicit* switch equation. The result is an implicit equation in which the outputs of the dependent storage elements $\dot{\boldsymbol{x}}_d$ and the output of the switches $\boldsymbol{T}_i$ into the JS are the unknowns. Accounting for the

field of storage elements, a second equation for these two unknowns can be set up. Both equations can be combined into a DAE for $\dot{\boldsymbol{x}}_d$ and $\boldsymbol{T}_i$. As a final result, implicitly given ARRs are obtained that relate known system inputs $\boldsymbol{u}$, measured output signals $\boldsymbol{v}_s^m$, $\dot{\boldsymbol{x}}_d$, and $\boldsymbol{T}_i$. Coefficients in the DAE system and in the ARRs are mode-dependent. The following sections present the steps of the outlined procedure.

$$\begin{bmatrix} \dot{\boldsymbol{x}}_i \\ \boldsymbol{z}_d \\ \boldsymbol{D}_o \\ \boldsymbol{T}_o \\ \boldsymbol{r} \end{bmatrix} = \left[\begin{array}{c|c|c|c|c|c} \mathbf{S}_{11} & \mathbf{S}_{12} & \mathbf{S}_{13} & \mathbf{S}_{14} & \mathbf{S}_{15} & \mathbf{S}_{16} \\ \hline -\mathbf{S}_{12}^T & \mathbf{S}_{22} & \mathbf{S}_{23} & \mathbf{S}_{24} & \mathbf{S}_{25} & \mathbf{S}_{26} \\ \hline -\mathbf{S}_{13}^T & -\mathbf{S}_{23}^T & \mathbf{S}_{33} & \mathbf{S}_{34} & \mathbf{S}_{35} & \mathbf{S}_{36} \\ \hline -\mathbf{S}_{14}^T & -\mathbf{S}_{24}^T & -\mathbf{S}_{34}^T & \mathbf{S}_{44} & \mathbf{S}_{45} & \mathbf{S}_{46} \\ \hline -\mathbf{S}_{15}^T & -\mathbf{S}_{25}^T & -\mathbf{S}_{35}^T & -\mathbf{S}_{45}^T & \mathbf{S}_{55} & \mathbf{S}_{56} \end{array}\right] \begin{bmatrix} \boldsymbol{z}_i \\ \dot{\boldsymbol{x}}_d \\ \boldsymbol{D}_i \\ \boldsymbol{T}_i \\ \boldsymbol{u} \\ \boldsymbol{v}_S^m \end{bmatrix} \tag{1}$$

Block diagram of a general BG extended by a field of switches and a field of inverted detectors

In this article, a DBG is used to set up ARRs for a switched linear system. As sensors provide measured signals, detectors in a DBG are in inverted causality. They deliver known signals into the model which are either efforts or flows. Following the notation used, for example, in Merzouki et al.[17] and Touati et al.,[18] effort detectors $\mathrm{D}e : e^m$ are replaced by a signal source $\mathrm{SS}e : e^m$ and flow detectors $\mathrm{D}e : f^m$ by a signal source $\mathrm{SS}f : f^m$. All such measured signals into the DBG are collected into a vector $\boldsymbol{v}_s^m$. Power variables at junctions with a detector attached are summed up, which yields a residual that is close to zero when the engineering system is faultless. Otherwise, the input into a detector is a residual that is significantly different from zero and thus may serve as a fault indicator. All residuals are composed into a vector $\boldsymbol{r}$. Switches may be controlled such as transistors or commutate autonomously such as diodes. The external signals affecting the discrete state of the controlled switches are collected into a function $\boldsymbol{\sigma}(t)$. All n_s discrete switch states $m_i(t)$, $i = 1, \ldots, n_s$, are collected into a vector $\boldsymbol{m}(t)$. Between two consecutive discrete switching events, switch states are constant. In a mode of operation, the continuous state of the system changes with time.

All storage elements in the DBG may take derivative causality. If the assignment of derivative causality results in a causal conflict, that is, a storage element cannot accept derivative causality, then a remedy may be to add another sensor if a measurement at the desired location is physically possible. For a behavioural linear BG model with storages in preferred integral causality and some storage elements retaining derivative causality, Rosenberg[19] has shown that the state variables of the dependent storages can be eliminated. Accordingly, for DBGs with storage elements in preferred derivative causality and a minimum number of storages in integral causality, the state variables of the latter ones can be eliminated. Therefore, it can be justified to assume that all storage elements in the DBG of a linear model are in derivative causality. The assumption makes the subsequent matrix-based approach more concise.

Setting up ARRs

The grouping of elements into fields is expressed by equation (1)

Because of the assumption that there are no storage elements in integral causality, that is, all storage elements can take derivative causality in the DBG, the equations in equation (1) simplify

$$\boldsymbol{z}_d = \mathbf{S}_{23}\boldsymbol{D}_i + \mathbf{S}_{24}\boldsymbol{T}_i + \mathbf{S}_{25}\boldsymbol{u} + \mathbf{S}_{26}\boldsymbol{v}_s^m \tag{2}$$

$$\boldsymbol{D}_o = -\mathbf{S}_{23}^T\dot{\boldsymbol{x}}_d + \mathbf{S}_{33}\boldsymbol{D}_i + \mathbf{S}_{34}\boldsymbol{T}_i + \mathbf{S}_{35}\boldsymbol{u} + \mathbf{S}_{36}\boldsymbol{v}_s^m \tag{3}$$

$$\boldsymbol{T}_o = -\mathbf{S}_{24}^T\dot{\boldsymbol{x}}_d - \mathbf{S}_{34}^T\mathbf{D}_i + \mathbf{S}_{44}\boldsymbol{T}_i + \mathbf{S}_{45}\boldsymbol{u} + \mathbf{S}_{46}\boldsymbol{v}_s^m \tag{4}$$

Accordingly, the equation for the vector of residuals, $\boldsymbol{r}$, reads

$$\boldsymbol{r} = -\mathbf{S}_{25}^T\dot{\boldsymbol{x}}_d - \mathbf{S}_{35}^T\boldsymbol{D}_i - \mathbf{S}_{45}^T\boldsymbol{T}_i + \mathbf{S}_{55}\boldsymbol{u} + \mathbf{S}_{56}\boldsymbol{v}_s^m \tag{5}$$

In equation (5), variables $\dot{\boldsymbol{x}}_d$, $\boldsymbol{D}_i$, and $\boldsymbol{T}_i$ must be expressed by known signals. The inputs and output of the resistive field are related by a matrix $\mathbf{L}$

$$\boldsymbol{D}_i = \mathbf{L}\boldsymbol{D}_o \tag{6}$$

Substituting equation (6) into equation (3) yields

$$(\mathbf{I} - \mathbf{S}_{33}\mathbf{L})\boldsymbol{D}_o = -\mathbf{S}_{23}^T\dot{\boldsymbol{x}}_d + \mathbf{S}_{34}\boldsymbol{T}_i + \mathbf{S}_{35}\boldsymbol{u} + \mathbf{S}_{36}\boldsymbol{v}_s^m \tag{7}$$

where $\mathbf{I}$ denotes an identity matrix of appropriate dimensions. Assuming that $(\mathbf{I} - \mathbf{S}_{33}\mathbf{L})$ can be inverted, then equations (6) and (4), respectively, read

$$\boldsymbol{D}_i = -\mathbf{H}\mathbf{S}_{23}^T\dot{\boldsymbol{x}}_d + \mathbf{H}\mathbf{S}_{34}\boldsymbol{T}_i + \mathbf{H}\mathbf{S}_{35}\boldsymbol{u} + \mathbf{H}\mathbf{S}_{36}\boldsymbol{v}_s^m \tag{8}$$

$$\begin{aligned}\boldsymbol{T}_o = &-(\mathbf{S}_{24}^T - \mathbf{S}_{34}^T\mathbf{H}\mathbf{S}_{23}^T)\dot{\mathbf{x}}_d + (\mathbf{S}_{44} - \mathbf{S}_{34}^T\mathbf{H}\mathbf{S}_{34})\mathbf{T}_i \\ &+ (\mathbf{S}_{45} - \mathbf{S}_{34}^T\mathbf{H}\mathbf{S}_{35})\boldsymbol{u} + (\mathbf{S}_{46} - \mathbf{S}_{34}^T\mathbf{H}\mathbf{S}_{36})\boldsymbol{v}_s^m\end{aligned} \tag{9}$$

where $\mathbf{H} := \mathbf{L}(\mathbf{I} - \mathbf{S}_{33}\mathbf{L})^{-1}$ ($\mathbf{H}$ exists in case $\mathbf{L}$ is a symmetric and positive definite matrix[3]).

The switches are assumed to be ideal, and their commutation is expressed by an *implicit* equation that holds independently of their causality

$$\mathbf{M}\mathbf{T}_o + \bar{\mathbf{M}}\mathbf{T}_i = \mathbf{0} \tag{10}$$

where $\mathbf{M}$ is a diagonal matrix with entries $m_{jj} \in \{1, 0\}$, $j = 1, \ldots, n_s$, and $\bar{\mathbf{M}} := \mathbf{I} - \mathbf{M}$.

That is, in the DBG, actual switch states are not expressed by the causality assigned to switch ports. In this article, switches are denoted by the often used but non-standard symbol $\mathrm{Sw} : m$. Their actual state is accounted for by $m \in \{0, 1\}$. Actually, the used non-standard symbol $\mathrm{S}w : m$ is meant to be generic. It may stand for an ideal switch as well as a non-ideal one. By the way, the half arrow added to the bonds of a BG also does not express the actual direction of the power flow but a reference direction.

The equation of the switches can be used to eliminate $\boldsymbol{T}_o$ in equation (9), which yields an implicit equation for $\dot{\boldsymbol{x}}_d$

$$\begin{aligned}\underbrace{\mathbf{M}(\mathbf{S}_{24}^T - \mathbf{S}_{34}^T\mathbf{H}\mathbf{S}_{23}^T)}_{\mathbf{M}_1}\dot{\boldsymbol{x}}_d = {} & \underbrace{[\bar{\mathbf{M}} + \mathbf{M}(\mathbf{S}_{44} - \mathbf{S}_{34}^T\mathbf{H}\mathbf{S}_{34})]}_{\mathbf{M}_2}\boldsymbol{T} \\ & + \underbrace{\mathbf{M}(\mathbf{S}_{45} - \mathbf{S}_{34}^T\mathbf{H}\mathbf{S}_{35})}_{\mathbf{M}_3}\mathbf{u} \\ & + \underbrace{\mathbf{M}(\mathbf{S}_{46} - \mathbf{S}_{34}^T\mathbf{H}\mathbf{S}_{36})}_{\mathbf{M}_4}\boldsymbol{v}_{si}^m\end{aligned} \tag{11}$$

This is an equation with the two unknowns $\dot{\boldsymbol{x}}_d$ and $\boldsymbol{T}_i$. Another equation for these unknowns can be obtained using the linear constitutive equations of the storage elements

$$\boldsymbol{z}_d = \mathbf{F}_d\boldsymbol{x}_d \tag{12}$$

where $\mathbf{F}_d$ is a diagonal matrix in case all storage elements are one-port elements. Substituting equation (2) into equation (12), observing equation (8) and differentiating the result with respect to time gives

$$\mathbf{F}_d\dot{\boldsymbol{x}}_d = \mathbf{S}_{23}\dot{\boldsymbol{D}}_i + \mathbf{S}_{24}\dot{\boldsymbol{T}}_i + \mathbf{S}_{25}\dot{\boldsymbol{u}} + \mathbf{S}_{26}\dot{\boldsymbol{v}}_s^m \tag{13}$$

$$\begin{aligned}= {} & -\underbrace{\mathbf{S}_{23}\mathbf{H}\mathbf{S}_{23}^T}_{\mathbf{N}_1}\ddot{\boldsymbol{x}}_d + \underbrace{[\mathbf{S}_{24} + \mathbf{S}_{23}\mathbf{H}\mathbf{S}_{24}]}_{\mathbf{N}_2}\boldsymbol{T}_i \\ & + \underbrace{[\mathbf{S}_{25} + \mathbf{S}_{23}\mathbf{H}\mathbf{S}_{35}]}_{\mathbf{N}_3}\dot{\boldsymbol{u}} \\ & + \underbrace{[\mathbf{S}_{26} + \mathbf{S}_{23}\mathbf{H}\mathbf{S}_{36}]}_{\mathbf{N}_4}\dot{\boldsymbol{v}}_s^m\end{aligned} \tag{14}$$

Equations (11) and (14) constitute a DAE system for $[\dot{\boldsymbol{x}}_d^T\ \boldsymbol{T}_i^T]^T$ for all modes of operation as the coefficients of the matrices depend on the discrete switch states

$$\begin{aligned}\begin{bmatrix}\mathbf{0} & \mathbf{0}\\ \mathbf{N}_1 & -\mathbf{N}_2\end{bmatrix}\frac{d}{dt}\begin{bmatrix}\dot{\boldsymbol{x}}_d\\ \boldsymbol{T}_i\end{bmatrix} = {} & \begin{bmatrix}-\mathbf{M}_1 & \mathbf{M}_2\\ -\mathbf{F}_d & \mathbf{0}\end{bmatrix}\begin{bmatrix}\dot{\boldsymbol{x}}_d\\ \boldsymbol{T}_i\end{bmatrix} + \begin{bmatrix}\mathbf{M}_3\\ \mathbf{0}\end{bmatrix}\boldsymbol{u} \\ & + \begin{bmatrix}\mathbf{0}\\ \mathbf{N}_3\end{bmatrix}\dot{\boldsymbol{u}} \\ & + \begin{bmatrix}\mathbf{M}_4\\ \mathbf{0}\end{bmatrix}\boldsymbol{v}_s^m + \begin{bmatrix}\mathbf{0}\\ \mathbf{N}_4\end{bmatrix}\dot{\boldsymbol{v}}_s^m\end{aligned} \tag{15}$$

Now, assume that the initial configuration of switch states and $\boldsymbol{T}_i(0)$ are known when the monitoring of a physical system starts. When an industrial system is set into operation, it is known which sources and which system components are connected and which ones are switched off. It is known whether a clutch in an electromechanical drive is engaged or disengaged at start time, or which transistors in an electronic circuit are closed and which ones are not when the system is switched on. For such a known initial switch configuration $\boldsymbol{T}_i(0) = 0$. Then, equation (11) provides $\dot{\boldsymbol{x}}_d(0)$. With these initial values equation (15) can be solved, and finally, an evaluation of equation (5) observing equation (8) yields the residuals. The numerical computation can be carried out simultaneously with the measuring of signals as the numerical integration algorithm using past values from a sliding time window only needs to perform some few time steps until new measured values are provided. If a mode change due to the commutation of some switches is encountered, the time instant is to be determined and the algorithm needs a fresh start with new initial conditions.

Unique mode-dependent state equations

In the case of a fault-free system, residuals vanish, that is, $\boldsymbol{r} = 0$. Substitution of equation (8) into equation (5) gives

$$\begin{aligned}\underbrace{[\mathbf{S}_{25}^T - \mathbf{S}_{35}^T\mathbf{H}\mathbf{S}_{23}^T]}_{\mathbf{Q}_1}\dot{\boldsymbol{x}}_d = {} & -\underbrace{[\mathbf{S}_{45}^T + \mathbf{S}_{35}^T\mathbf{H}\mathbf{S}_{34}]}_{\mathbf{Q}_2}\boldsymbol{T}_i \\ & + \underbrace{[\mathbf{S}_{55} - \boldsymbol{v}_{35}^T\mathbf{H}\mathbf{S}_{35}]}_{\mathbf{Q}_3}\boldsymbol{u} \\ & + \underbrace{[\mathbf{S}_{56} - \mathbf{S}_{35}^T\mathbf{H}\mathbf{S}_{36}]}_{\mathbf{Q}_4}\boldsymbol{v}_s^m\end{aligned} \tag{16}$$

Equations (11), (14), and (16) constitute an implicit linear algebraic set of equations with mode-dependent coefficients from which implicit state equation can be deduced for all modes of operation

$$\begin{aligned}\begin{bmatrix}\mathbf{M}_1 & -\mathbf{M}_2 & -\mathbf{M}_4\\ \mathbf{Q}_1 & \mathbf{Q}_2 & -\mathbf{Q}_4\\ \mathbf{N}_1 & -\mathbf{N}_2 & -\mathbf{N}_4\end{bmatrix}\begin{bmatrix}\dot{\boldsymbol{x}}_d\\ \boldsymbol{T}_i\\ \boldsymbol{v}_s^m\end{bmatrix} = {} & \begin{bmatrix}\mathbf{0}\\ \mathbf{0}\\ -\mathbf{F}_d\end{bmatrix}\boldsymbol{x}_d \\ & + \begin{bmatrix}\mathbf{M}_3\\ \mathbf{Q}_3\\ \mathbf{N}_3\end{bmatrix}[\boldsymbol{u}]\end{aligned} \tag{17}$$

Illustrative examples

A software implementation of the general matrix-based procedure presented in the previous section may be used to automatically set up mode-dependent ARRs for large-scale mode-switching LTI models and to obtain implicit state equations that hold for all modes of operation. If a model is of moderate size, one can manually directly derive equations from a DBG by following causal paths. In the sequel, in order to avoid a handling with matrices of large dimensions and to keep the presentation easy to survey, small illustrative examples are considered. The equations derived from a DBG are reformulated so that one can see how the matrices in the general approach actually look like in the examples.

A DC motor drive with a load

Figure 2 shows a diagram of a DC motor that obtains its input voltage from a buck converter.

The drive includes three switching devices, namely, the controlled transistor, the autonomously switching diode, and the mechanical clutch. As in Buisson et al.,[3] all three

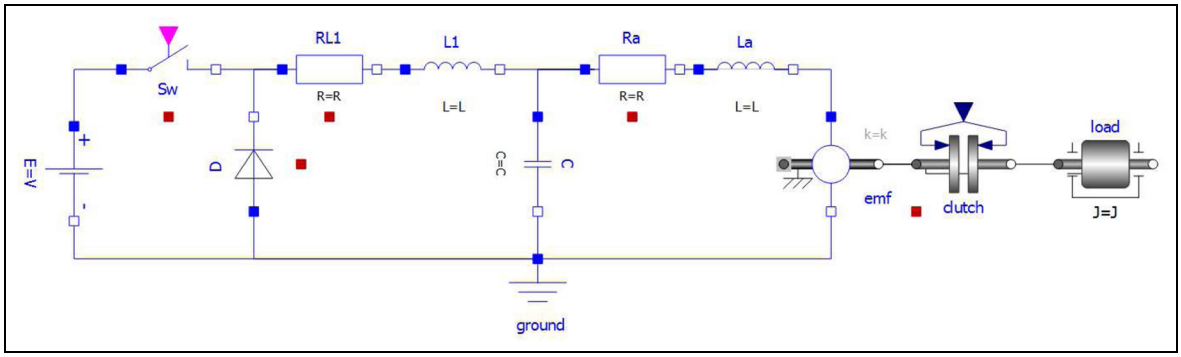

Figure 2. DC motor drive with a load.

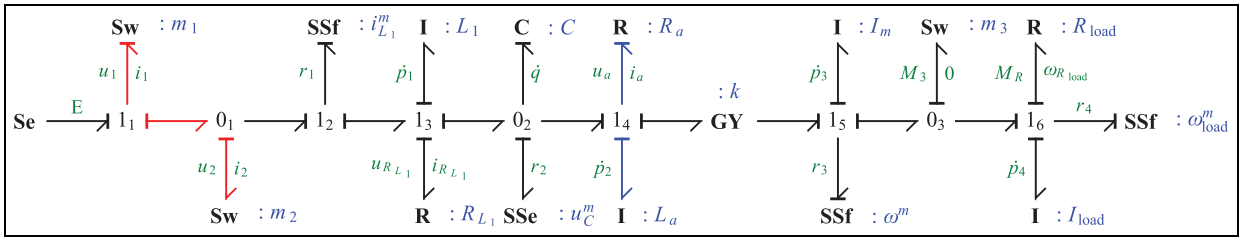

Figure 3. Diagnostic bond graph of the DC motor drive.

of them are modelled as ideal switches. Figure 3 displays a DBG of the electromechanical system.

Annotated power variables denoting measured quantities carry a superscript m. The causal path between the two left-side switches highlighted in red colour indicates that the port variables of the two switches are algebraically dependent.

Direct deduction of equations. The subsequent equations are directly read out from the DBG in Figure 3. The meaning of variables and parameters is indicated by the DBG

$$u_1 = E - u_2 \tag{18}$$

$$i_2 = i_1 - i_{L_1}^m \tag{19}$$

$$u_{R_{L_1}} = R_{L_1} i_{R_{L_1}} \tag{20}$$

$$i_{R_{L_1}} = i_{L_1}^m \tag{21}$$

$$i_a = \frac{1}{R_a} u_a \tag{22}$$

$$M_R = R_{load} \omega_{load}^m \tag{23}$$

$$\omega_3 = \omega^m - \omega_{load}^m \tag{24}$$

$$\dot{p}_1 = L_1 \frac{d}{dt} i_{L_1}^m \tag{25}$$

$$\dot{p}_3 = I_m \dot{\omega}^m \tag{26}$$

$$\dot{p}_4 = I_{load} \dot{\omega}_{load}^m \tag{27}$$

$$\dot{q} = C \dot{u}_C^m \tag{28}$$

$$\text{ARR}_1: \quad 1_2: \quad r_1 = u_2 - L_1 \frac{d}{dt} i_{L_1}^m - R_{L_1} i_{L_1}^m - u_C^m \tag{29}$$

$$\text{ARR}_2: \quad 0_2: \quad r_2 = i_{L_1}^m - C \dot{u}_C^m - i_a \tag{30}$$

$$\text{ARR}_3: \quad 1_5: \quad r_3 = k i_a - \dot{p}_3 - M_3 \tag{31}$$

$$\text{ARR}_4: \quad 1_6: \quad r_4 = M_3 - \dot{p}_4 - R_{load} \omega_{load}^m \tag{32}$$

Furthermore, there is a causal path highlighted in blue colour between the inductor I : L_a and the resistor R : R_a of the armature winding, which means that matrix $-\mathbf{S}_{23}^T$ in equation (1) does not vanish. With the summation of efforts at junction 1_4, this causal path contributes the two equations

$$i_a = \frac{1}{R_a} (u_C^m - \dot{p}_2 - k \omega^m) \tag{33}$$

$$\dot{p}_2 = L_a \frac{d}{dt} i_a \tag{34}$$

that can be combined into an ODE for i_a

$$L_a \frac{d}{dt} i_a + R_a i_a = u_C^m - k \omega^m \tag{35}$$

By looking at the ARRs, it can be seen that ARR_1 is mode-dependent as it depends on u_2, which is a port variable of switch Sw : m_2. Residuals ARR_3 and ARR_4 are also mode-dependent as they do depend on switch Sw : m_3 representing the clutch. In case the clutch is disengaged, clearly, $M_3 = 0$, $\omega^m \neq \omega_{load}^m$, and residuals r_3, r_4 are independent

$$r_3 = ki_a - I_m\dot{\omega}^m \tag{36}$$

$$r_4 = -I_{load}\dot{\omega}^m_{load} - R_{load}\omega^m_{load} \tag{37}$$

When the clutch engages, load I : I_{load} and the motor do have the same measured angular velocity ω^m. The discs of the clutch sticking together can be considered as one rigid body. The two storage elements I : I_m and I : I_{load} are rigidly connected and are thus dependent. As both sensors measure the same angular velocity, one of them is redundant and residuals r_3, r_4 are algebraically dependent. They are related by the constraint

$$r_3 + r_4 = ki_a - (I_m + I_{load})\dot{\omega}^m - R_{load}\omega^m \tag{38}$$

The case of two storage elements becoming dependent by the closing of a switch will be considered in the second example. In the following, the study of the electromechanical drive assumes that the clutch is permanently engaged. That is, $\omega^m_{load} = \omega^m$. Accordingly, switch Sw : m_3 can be omitted and one detector of the angular velocity is sufficient. Residual r_3 then becomes mode-independent and reads

$$r_3 = ki_a - (I_m + I_{load})\dot{\omega}^m - R_{load}\omega^m \tag{39}$$

The two ideal switches Sw : m_1 and Sw : m_2 in the converter model are described by the following two implicit algebraic equations

$$\begin{aligned} 0 &= m_1u_1 + \bar{m}_1i_1 \\ &= m_1(E - u_2) + \bar{m}_1i^m_{L_1} \end{aligned} \tag{40}$$

$$\begin{aligned} 0 &= m_2i_2 + \bar{m}_2u_2 \\ &= m_2(i_1 - i^m_{L_1}) + \bar{m}_2u_2 \end{aligned} \tag{41}$$

Elimination of switch variable i_1 yields

$$(m_1\bar{m}_2 + \bar{m}_1m_2)u_2 = m_1\bar{m}_2E + \bar{m}_1\bar{m}_2i^m_{L_1} \tag{42}$$

As the two switches in the buck converter model commutate oppositely, $m_2 = \bar{m}_1$ holds so that equation (42) simplifies to

$$u_2 = m_1\bar{m}_2E = m_1E \tag{43}$$

and ARR_1 (29) thus reads

$$r_1 = m_1E - L_1\frac{d}{dt}i^m_{L_1} - R_{L_1}i^m_{L_1} - u^m_C \tag{44}$$

That is, for this example, the solution of two linear algebraic equations enables to evaluate the ARRs. This is also reflected by the causal path highlighted in red colour in the left part of the DBG. The opposite commutation of the two switches would only reverse the causal strokes on the causal path between them.

Equations of the matrix-based procedure. In the following, the above equations directly obtained from the DBG in Figure 3 are reformulated so that it can be seen of what form the equations of the matrix-based procedure presented in the previous section are in this example. First, reformulation of equations (18) and (19) leads to equation (4)

$$\begin{aligned} \underbrace{\begin{bmatrix} u_1 \\ i_2 \end{bmatrix}}_{\boldsymbol{T}_o} &= \underbrace{\begin{bmatrix} 0 & -1 \\ 1 & 0 \end{bmatrix}}_{\mathbf{S}_{44}} \underbrace{\begin{bmatrix} i_1 \\ u_2 \end{bmatrix}}_{\boldsymbol{T}_i} + \underbrace{\begin{bmatrix} 1 \\ 0 \end{bmatrix}}_{\mathbf{S}_{45}} \underbrace{[E]}_{\boldsymbol{u}} \\ &\quad + \underbrace{\begin{bmatrix} 0 & 0 & 0 \\ -1 & 0 & 0 \end{bmatrix}}_{\mathbf{S}_{46}} \underbrace{\begin{bmatrix} i^m_{L_1} \\ u^m_C \\ \omega^m \end{bmatrix}}_{\boldsymbol{v}^m_s} \end{aligned} \tag{45}$$

Rewriting equations (20)–(23), equation (35) gives equation (3)

$$\begin{aligned} \underbrace{\begin{bmatrix} i_{R_{L_1}} \\ u_a \\ \omega_{R_{load}} \end{bmatrix}}_{\boldsymbol{D}_o} &= \underbrace{\begin{bmatrix} 0 & 0 & 0 & 0 & 0 \\ 0 & -1 & 0 & 0 & 0 \\ 0 & 0 & 0 & 0 & 0 \end{bmatrix}}_{-\mathbf{S}^T_{23}} \underbrace{\begin{bmatrix} \dot{p}_1 \\ \dot{p}_2 \\ \dot{p}_3 \\ \dot{p}_4 \\ \dot{q} \end{bmatrix}}_{\dot{\boldsymbol{x}}_d} \\ &\quad + \underbrace{\begin{bmatrix} 1 & 0 & 0 \\ 0 & 1 & -k \\ 0 & 0 & 1 \end{bmatrix}}_{\mathbf{S}_{36}} \underbrace{\begin{bmatrix} i^m_{L_1} \\ u^m_C \\ \omega^m \end{bmatrix}}_{\boldsymbol{v}^m_s} \end{aligned} \tag{46}$$

Equations (25)–(28) and (34) may be written in the form

$$\begin{aligned} &\underbrace{\begin{bmatrix} 1/L_1 & 0 & 0 & 0 & 0 \\ 0 & 1/L_a & 0 & 0 & 0 \\ 0 & 0 & 1/I_m & 0 & 0 \\ 0 & 0 & 0 & 1/I_{load} & 0 \\ 0 & 0 & 0 & 0 & 1/C \end{bmatrix}}_{\mathbf{F}_d} \underbrace{\begin{bmatrix} \dot{p}_1 \\ \dot{p}_2 \\ \dot{p}_3 \\ \dot{p}_4 \\ \dot{q} \end{bmatrix}}_{\dot{\boldsymbol{x}}_d} = \\ &\underbrace{\begin{bmatrix} 0 & 0 & 0 \\ 0 & 1 & 0 \\ 0 & 0 & 0 \\ 0 & 0 & 0 \\ 0 & 0 & 0 \end{bmatrix}}_{\mathbf{S}_{23}} \underbrace{\frac{d}{dt}\begin{bmatrix} u_{R_{L_1}} \\ i_a \\ M_R \end{bmatrix}}_{\dot{\boldsymbol{D}}_i} + \underbrace{\begin{bmatrix} 1 & 0 & 0 \\ 0 & 0 & 0 \\ 0 & 0 & 1 \\ 0 & 0 & 1 \\ 0 & 1 & 0 \end{bmatrix}}_{\mathbf{S}_{26}} \underbrace{\frac{d}{dt}\begin{bmatrix} i^m_{L_1} \\ u^m_C \\ \omega^m \end{bmatrix}}_{\dot{\boldsymbol{v}}^m_s} \end{aligned} \tag{47}$$

The result is equation (13) differentiated with respect to time. The implicit switch equations read

$$\underbrace{\begin{bmatrix} m_1 & 0 \\ 0 & m_2 \end{bmatrix}}_{\mathbf{M}} \underbrace{\begin{bmatrix} u_1 \\ i_2 \end{bmatrix}}_{\boldsymbol{T}_o} + \underbrace{\begin{bmatrix} \bar{m}_1 & 0 \\ 0 & \bar{m}_2 \end{bmatrix}}_{\bar{\mathbf{M}}} \underbrace{\begin{bmatrix} i_1 \\ u_2 \end{bmatrix}}_{\boldsymbol{T}_i} = 0 \tag{48}$$

Substitution of equation (45) into equation (48) gives

$$0 = (\bar{\mathbf{M}} + \mathbf{M}\mathbf{S}_{44})\boldsymbol{T}_i + \mathbf{M}\mathbf{S}_{45}\boldsymbol{u} + \mathbf{M}\mathbf{S}_{46}\boldsymbol{v}^m_s \tag{49}$$

For this example, equation (11) reduces to an algebraic equation for $\boldsymbol{T}_i$. Furthermore, equation (6) reads

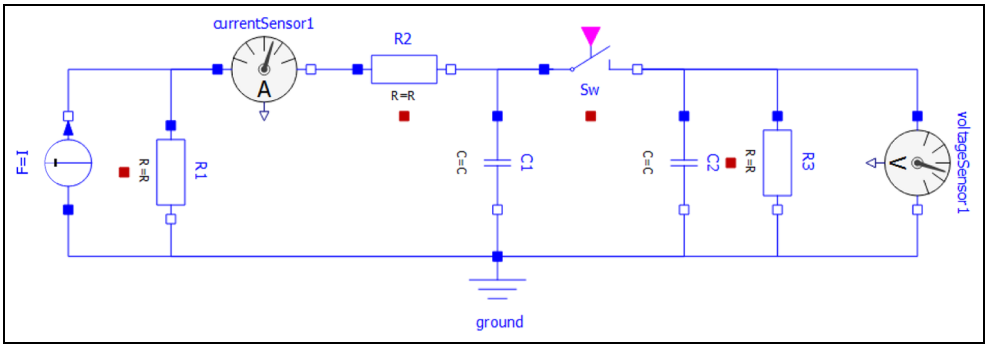

Figure 4. Circuit with an ideal switch Sw connecting two capacitors.

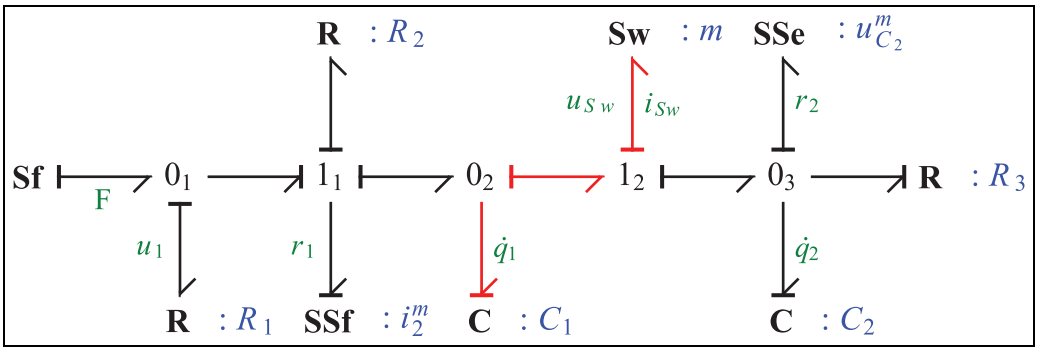

Figure 5. DBG of the circuit with two capacitors.

$$\boldsymbol{D}_i = \underbrace{\mathrm{diag}(R_{L_1}\ 1/R_a\ R_{load})}_{\mathbf{L}}\boldsymbol{D}_o \tag{50}$$

With equation (46) into equation (50) and the result into equation (47), one obtains an ODE for $\boldsymbol{x}_d$. Finally, equation (5) for the residuals reads

$$\underbrace{\begin{bmatrix} r_1 \\ r_2 \\ r_3 \end{bmatrix}}_{\boldsymbol{r}} = \underbrace{\begin{bmatrix} 0 & 1 \\ 0 & 0 \\ 0 & 0 \end{bmatrix}}_{-\mathbf{S}^T_{45}} \underbrace{\begin{bmatrix} i_1 \\ u_2 \end{bmatrix}}_{\boldsymbol{T}_i} + \underbrace{\begin{bmatrix} -1 & 0 & 0 & 0 & 0 \\ 0 & 0 & 0 & 0 & -1 \\ 0 & 0 & -1 & -1 & 0 \end{bmatrix}}_{-\mathbf{S}^T_{25}} \underbrace{\begin{bmatrix} \dot{p}_1 \\ \dot{p}_2 \\ \dot{p}_3 \\ \dot{p}_4 \\ \dot{q} \end{bmatrix}}_{\dot{\boldsymbol{x}}_d}$$
$$+ \underbrace{\begin{bmatrix} 0 & -1 & 0 \\ 1 & 0 & 0 \\ 0 & 0 & 0 \end{bmatrix}}_{\mathbf{S}_{55}} \underbrace{\begin{bmatrix} i^m_{L_1} \\ u^m_C \\ \omega^m \end{bmatrix}}_{\boldsymbol{v}^m_S} + \underbrace{\begin{bmatrix} -1 & 0 & 0 \\ 0 & -1 & 0 \\ 0 & k & -1 \end{bmatrix}}_{-\mathbf{S}^T_{35}} \underbrace{\begin{bmatrix} u_{R_{L_1}} \\ i_a \\ M_R \end{bmatrix}}_{\boldsymbol{D}_i} \tag{51}$$

Substituting equation (46) into equation (50) and the result into equation (5) gives the residual vector, $\boldsymbol{r}$, as a linear function of $\boldsymbol{T}_i$, $\dot{\boldsymbol{x}}_d$, and $\boldsymbol{v}^m_S$.

An all mode implicit state space model. If there is no fault in the physical system, then the residuals vanish. Assuming that the clutch is permanently closed, then neglecting of elements R_{L_1}, C, and L_a in the ARRs leads to the following implicit state space equations

$$\dot{p}_1 = m_1 E - R_a \frac{p_1}{L_1} - k\frac{p_3}{I_m} \tag{52}$$

$$\dot{p}_3 + \dot{p}_4 = k\frac{p_1}{L_1} - R_{load}\frac{p_3}{I_m} \tag{53}$$

$$0 = \frac{p_3}{I_m} - \frac{p_4}{I_{load}} \tag{54}$$

The resulting DAE holds for the two modes of operation determined by the discrete state m_1 of the controlled switch Sw : m_1 and is identical to the one given in Buisson et al.[3] Differentiating equation (54) once reduces the DAE into an ODE for $[p_1\ p_3]$. That is, the resulting DAE system is of index 1.

However, in contrast to the approach in Buisson et al.,[3] the DAE system is not deduced from the state space model of a reference configuration, but obtained directly from a single DBG with fixed causalities.

An ideal switch connecting two capacitors

In this section, it is shown that the presented approach to the generation of mode-dependent ARRs and a unique implicit state equation from a fixed-causality DBG is also applicable to systems in which the closing of an ideal switch leads to an algebraic dependency between the states of two storage elements. If this dependency would be expressed by a change of causal strokes in a DBG of the system, then one of the two

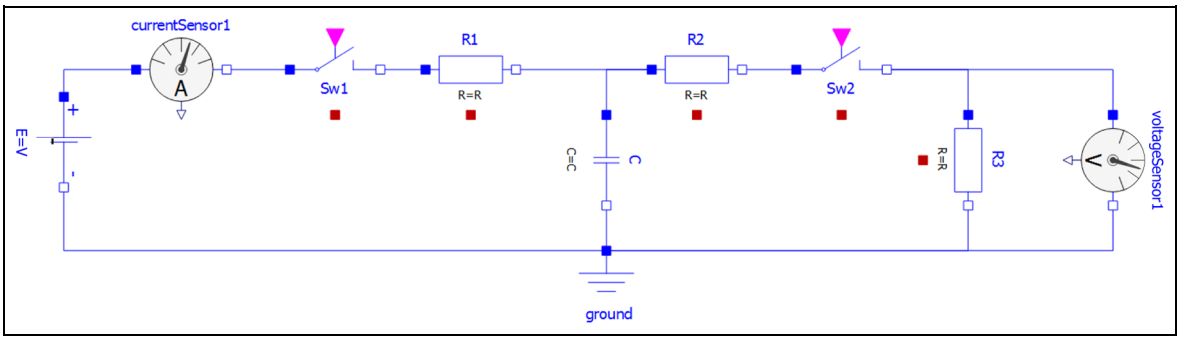

Figure 6. Two independent switches.

storage elements would turn from initially assigned derivative causality into integral causality. In contrast, the presented approach stays with fixed causalities and makes use of an *implicit* equation for the *ideal* switches in the model.

As an example, Figure 4 displays the schematic of the well-known circuit example with two capacitors in parallel.[20] This example is interesting as a closing of the ideal switch leads to a higher index problem. That is, the index of the DAE system is mode-dependent.

Figure 5 displays a DBG of the circuit in Figure 4.

As can be seen from Figure 5, the two capacitors are in static derivative causality, and the detectors are in inverse causality. Accordingly, the output of the switch is its effort. Whether the switch is on or off is implicitly taken into account by the value of its discrete state variable m. Moreover, the causal path $\mathrm{Sw} : m - \mathrm{C} : C_1$, highlighted in red colour, implicitly indicates the dependency between the two capacitors. If the closing of the switch would be accounted by a change of causal strokes, then a causal path between the capacitors would result.

Direct deduction of equations. Inspection of the DBG in Figure 5 immediately yields the following equations

$$i_{\mathrm{Sw}} = -\dot{q}_1 + i_2^m \tag{55}$$

$$\dot{q}_1 = C_1(\dot{u}_{\mathrm{Sw}} + \dot{u}_{C_2}^m) \tag{56}$$

$$\dot{q}_2 = C_2 \dot{u}_{C_2}^m \tag{57}$$

$$\mathrm{ARR}_1 : \quad 1_1 : \quad r_1 = R_1(F - i_2^m) - R_2 i_2^m - \frac{1}{C_1} q_1 \tag{58}$$

$$\mathrm{ARR}_2 : \quad 0_3 : \quad r_2 = i_{\mathrm{Sw}} - \dot{q}_2 - \frac{1}{R_3}\frac{q_2}{C_2} \tag{59}$$

The ideal switch is described by the implicit equation

$$0 = m i_{\mathrm{Sw}} + \bar{m} u_{\mathrm{Sw}} \tag{60}$$

Equations of the matrix-based procedure. Reformulation of equation (55) and substitution into the switch equation yields

$$\underbrace{[m]}_{\mathbf{M}} \underbrace{[1 \quad 0]}_{\mathbf{S}_{24}^T} \underbrace{\begin{bmatrix} \dot{q}_1 \\ \dot{q}_2 \end{bmatrix}}_{\dot{\boldsymbol{x}}_d} = \underbrace{[\bar{m}]}_{\mathbf{M}} \underbrace{[u_{\mathrm{Sw}}]}_{\mathbf{T}_i} + \underbrace{[m]}_{\mathbf{M}} \underbrace{[1 \quad 0]}_{\mathbf{S}_{46}} \underbrace{\begin{bmatrix} i_2^m \\ u_{C_2}^m \end{bmatrix}}_{\boldsymbol{v}_s^m} \tag{61}$$

Combining equations (56) and (57) gives equation (13)

$$\underbrace{\begin{bmatrix} 1/C_1 & 0 \\ 0 & 1/C_2 \end{bmatrix}}_{\mathbf{F}_d} \underbrace{\begin{bmatrix} \dot{q}_1 \\ \dot{q}_2 \end{bmatrix}}_{\dot{\boldsymbol{x}}_d} = \underbrace{\begin{bmatrix} 1 \\ 0 \end{bmatrix}}_{\mathbf{S}_{24}} \underbrace{[\dot{u}_{\mathrm{Sw}}]}_{\dot{\boldsymbol{T}}_i} + \underbrace{\begin{bmatrix} 0 & 1 \\ 0 & 1 \end{bmatrix}}_{\mathbf{S}_{26}} \underbrace{\frac{d}{dt}}_{} \underbrace{\begin{bmatrix} i_2^m \\ u_{C_2}^m \end{bmatrix}}_{\dot{\boldsymbol{v}}_s^m} \tag{62}$$

Equations (61) and (62) may be combined into the DAE

$$\begin{bmatrix} \mathbf{M}\mathbf{S}_{24}^T & -\bar{\mathbf{M}} \\ \mathbf{0} & -\mathbf{S}_{24} \end{bmatrix} \begin{bmatrix} \ddot{\boldsymbol{x}}_d \\ \dot{\boldsymbol{T}}_i \end{bmatrix} = \begin{bmatrix} \mathbf{0} & \mathbf{0} \\ -\mathbf{F}_d & \mathbf{0} \end{bmatrix} \begin{bmatrix} \dot{\boldsymbol{x}}_d \\ \boldsymbol{T}_i \end{bmatrix} + \begin{bmatrix} \mathbf{M}\mathbf{S}_{46} \\ \mathbf{S}_{26} \end{bmatrix} [\dot{\boldsymbol{v}}_s^m] \tag{63}$$

In this simple case, substitution of equation (62) into equation (61) gives an ODE for $\mathbf{T}_i$

$$\mathbf{M}\mathbf{S}_{24}^T \mathbf{F}_d^{-1} \mathbf{S}_{24} \dot{\boldsymbol{T}}_i - \bar{\mathbf{M}} \boldsymbol{T}_i = \mathbf{M}\mathbf{S}_{46} \boldsymbol{v}_s^m - \mathbf{M}\mathbf{S}_{24}^T \mathbf{F}_d^{-1} \mathbf{S}_{26} \dot{\boldsymbol{v}}_s^m \tag{64}$$

For $m = 0$, this ODE reduces to $T_i = 0 = u_{\mathrm{sw}}$, that is, the switch is closed. For $m = 1$, the multiplication of matrices yields

$$c_1 \dot{T}_i = c_1 \dot{u}_{\mathrm{sw}} = i_2^m - c_1 \dot{u}_{c_2}^m \tag{65}$$

As the switch is open $i_2^m = \dot{q}_1 = c_1 \dot{u}_{c_1}$. Hence, the result is $u_{\mathrm{sw}} = u_{c_1} - u_{c_2}$ as to be expected. Finally, reformulation of the ARRs yields

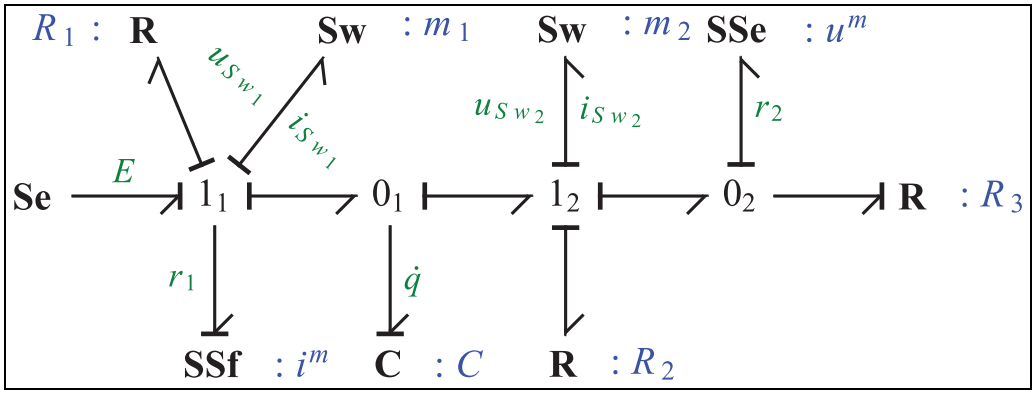

Figure 7. DBG of the circuit in Figure 6.

$$\underbrace{\begin{bmatrix} r_1 \\ r_2 \end{bmatrix}}_{\boldsymbol{r}} = \begin{bmatrix} 0 & 0 \\ -1 & -1 \end{bmatrix} \underbrace{\begin{bmatrix} \dot{q}_1 \\ \dot{q}_2 \end{bmatrix}}_{\dot{\boldsymbol{x}}_d} + \begin{bmatrix} -1 \\ 0 \end{bmatrix} \underbrace{[u_{sw}]}_{\boldsymbol{T}_i} + \begin{bmatrix} R_1 \\ 0 \end{bmatrix} \underbrace{[F]}_{u} + \begin{bmatrix} -R & -1 \\ 1 & -1/R_3 \end{bmatrix} \underbrace{\begin{bmatrix} i_2^m \\ u_{c_2}^m \end{bmatrix}}_{\boldsymbol{v}_s^m} \tag{66}$$

where $R = R_1 + R_2$.

An all mode implicit state space model. Again, an implicit DAE with mode-dependent parameters can be obtained from the ARRs if the residuals vanish. Reformulation yields the following unique implicit form for both modes of operation

$$\underbrace{\begin{bmatrix} 1 & 1 \\ 0 & m \end{bmatrix} \begin{bmatrix} \dot{q}_1 \\ \dot{q}_2 \end{bmatrix}}_{\dot{\boldsymbol{q}}} = \begin{bmatrix} -\frac{1}{RC_1} & -\frac{1}{R_3C_2} \\ -\frac{\bar{m}}{C_1} & \left(\bar{m} - \frac{m}{R_3}\right)\frac{1}{C_2} \end{bmatrix} \begin{bmatrix} q_1 \\ q_2 \end{bmatrix} + \begin{bmatrix} R_1/R \\ 0 \end{bmatrix} [F] \tag{67}$$

The differentiation index of equation (67) depends on mode m. For $m = 1$ (open switch), the matrix premultiplying $\dot{\boldsymbol{q}}$ is invertible. In this case, the index is zero. For $m = 0$ (closed switch), the second equation is an algebraic constraint which simply expresses that the voltage across both capacitors is the same. Differentiation of this constraint reduces the DAE system into an ODE. That is, in this mode, the DAE is of index 1. The problem in practice is that software such as OpenModelica does not perform index reduction during simulation. The computation just fails when the switch state m becomes zero.

Controlled independent switches

The third example illustrates the application of the approach to a simple circuit with two controlled independent switches. Figure 6 shows the circuit schematic.

Figure 7 displays a DBG with two detectors. The inverted causalities at the detector ports and the derivative causality at the storage port enforce an effort out causality at the switch ports independent of their state.

Summation of efforts at 1-junctions and flows at 0-junctions leads to the following equations

$$i_{sw_1} = i^m \tag{68}$$

$$r_1 = E - R_1 i^m - u_{sw_1} - u_c \tag{69}$$

$$\dot{q} = i^m - i_{sw_2} \tag{70}$$

$$u_c = R_2 i_{sw_2} + u_{sw_2} + u^m \tag{71}$$

The switches are described by the implicit equation

$$\begin{bmatrix} 0 \\ 0 \end{bmatrix} = \underbrace{\begin{bmatrix} m_1 & 0 \\ 0 & m_2 \end{bmatrix}}_{\mathbf{M}} \underbrace{\begin{bmatrix} u_{sw_1} \\ u_{sw_2} \end{bmatrix}}_{\boldsymbol{T}_i} + \underbrace{\begin{bmatrix} \bar{m}_1 & 0 \\ 0 & \bar{m}_2 \end{bmatrix}}_{\bar{\mathbf{M}}} \underbrace{\begin{bmatrix} i_{sw_1} \\ i_{sw_2} \end{bmatrix}}_{\boldsymbol{T}_o} \tag{72}$$

Reformulation of equations (68) and (70) gives

$$\underbrace{\begin{bmatrix} i_{sw_1} \\ i_{sw_2} \end{bmatrix}}_{\boldsymbol{T}_o} = \underbrace{\begin{bmatrix} 0 \\ -1 \end{bmatrix}}_{-\mathbf{S}_{24}^T} \underbrace{[\dot{q}]}_{\dot{x}_d} + \underbrace{\begin{bmatrix} 1 & 0 \\ 1 & 0 \end{bmatrix}}_{\mathbf{S}_{46}} \underbrace{\begin{bmatrix} i^m \\ u^m \end{bmatrix}}_{\boldsymbol{v}_s^m} \tag{73}$$

Substituting equation (73) into equation (72) yields

$$\bar{\mathbf{M}}\mathbf{S}_{24}^T \dot{x}_d = -\mathbf{M}\boldsymbol{T}_i + \bar{\mathbf{M}}\mathbf{S}_{46}\boldsymbol{v}_s^m \tag{74}$$

The state equation of the capacitor gives

$$\bar{m}_2 \frac{1}{c} q = (\bar{m}_2 - m_2 R_2) u_{sw_2} + \bar{m}_2 u^m \tag{75}$$

or

$$\bar{m}_2 \frac{1}{c} \dot{x}_d = [0 \;\; (\bar{m}_2 - m_2 R_2)] \dot{\boldsymbol{T}}_i + [0 \;\; 1] \dot{\boldsymbol{v}}_s^m \tag{76}$$

Finally, the equations for the residuals read

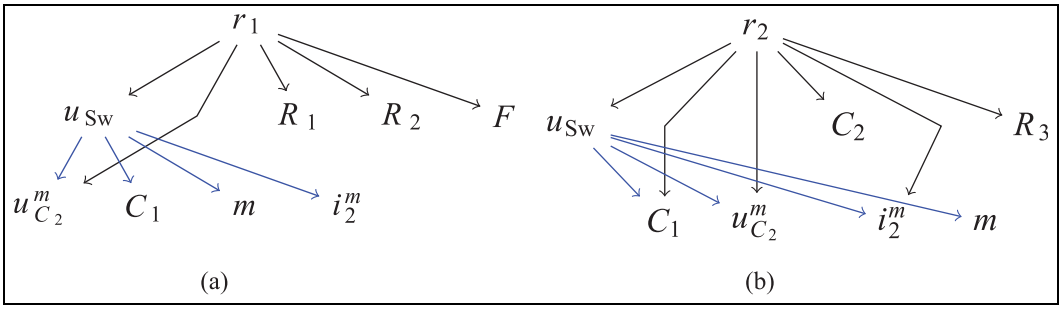

Figure 8. Dependency graph for residuals r_1, r_2 of the second example: (a) residual r_1 and (b) residual r_2.

$$\underbrace{\begin{bmatrix} r_1 \\ r_2 \end{bmatrix}}_{\boldsymbol{r}} = \begin{bmatrix} -R_1 \\ -1 \end{bmatrix} \underbrace{[\dot{q}]}_{\dot{x}_d} + \begin{bmatrix} -1 & -1 \\ 0 & 0 \end{bmatrix} \underbrace{\begin{bmatrix} u_{sw_1} \\ u_{sw_2} \end{bmatrix}}_{\boldsymbol{T}_i} + \begin{bmatrix} 0 \\ 1 \end{bmatrix} \underbrace{[E]}_{\boldsymbol{u}} + \begin{bmatrix} -R & -1 \\ -1 & -1/R_3 \end{bmatrix} \underbrace{\begin{bmatrix} i^m \\ u^m \end{bmatrix}}_{\boldsymbol{v}_s^m} \tag{77}$$

In the case of a fault-free circuit, one obtains the following state equation

$$\begin{aligned} \dot{q} &= i_{sw_1} - i_{sw_2} = [1 \; -1]\boldsymbol{T}_o \\ &= \frac{m_1}{m_1 R_1 - \bar{m}_1}\left(E - \frac{q}{C}\right) \\ &\quad - \frac{m_2}{m_2(R_2 + R_3) - \bar{m}_2}\frac{q}{C} \end{aligned} \tag{78}$$

which is valid for all four switch-state configurations. If both switches are open ($m_1 = m_2 = 0$), equation (78) correctly yields $\dot{q} = 0$.

Structural fault signature matrix

A structural fault signature matrix (FSM) reflects the dependency of ARRs from component parameters. If a residual r_i (column i of a FSM) exceeds a mode-dependent fault threshold thr_i^j, where j denotes the mode, then a fault is detected in that mode and at least one of the parameters included in the ARR taken into account in one row of the FSM is a fault candidate. For the circuit in Figure 4, residual r_1 reads

$$r_1 = -u_{\mathrm{sw}} - u_{C_2}^m - Ri_2^m + R_1 F \tag{79}$$

(cf. equation (66)). Substituting equation (56) into equation (55) and the result into the implicit switch equation (60) gives an implicit ODE for u_{sw}

$$mC_1\dot{u}_{\mathrm{sw}} - \bar{m}u_{\mathrm{sw}} = m\dot{i}_2^m - mC_1\dot{u}_{C_2}^m \tag{80}$$

Residual r_2 reads

$$r_2 = -(C_1\dot{u}_{\mathrm{sw}} + \dot{u}_{C_2}^m) - C_2\dot{u}_{C_2}^m + \dot{i}_2^m - \frac{1}{R_3}u_{C_2}^m \tag{81}$$

Table 1 shows the FSM for the second example.

The two additional columns on the right side of the table hold further information. Entries in the last but one column indicate the detectability of a fault. The last column keeps record of the isolability of a fault. As can be seen, all potential faults can be detected, but none, except a faulty capacitance, can be isolated with the given sensors. The last three rows of the FSM may be omitted if the current source $\mathrm{S}f : F$ and the sensors can be assumed to be fault free.

Table 1. Structural fault signature matrix of the circuit with two parallel capacitors and sensors Df : i_2^m and De : $u_{C_2}^m$ (Figure 4).

Component	ARR_1	ARR_2	D	I
R : R_1	1	0	1	0
R : R_2	1	0	1	0
C : C_1	1	1	1	0
Sw : m	1	1	1	0
C : C_2	0	1	1	0
R : R_3	0	1	1	0
Sf : F	1	0	1	0
Sensor of i_2^m	1	1	1	0
Sensor of $u_{C_2}^m$	1	1	1	0

In the presented approach, the vector of residuals, $\boldsymbol{r}$, depends on $\dot{\boldsymbol{x}}_d$, $\boldsymbol{T}_i$ which are given by a DAE (cf. equation (15)). Accordingly, to set up an FSM, equations of the residuals and the DAE system are to be inspected with regard to parameters and measured variables (sensor outputs). Dependencies may be captured in a dependency graph. Figure 8 displays the dependency graphs for residuals r_1, r_2 (cf. Figure 5).

Non-ideal switches

A slight modification of the implicit equation of an ideal switch allows to apply the approach presented in section 'Formal matrix-based approach' in the case that some of the switches in a model are to be considered non-ideal. For these switches, the plus sign in equation (60) is replaced by a minus sign and their discrete state is allowed to take values ϵ or $1 - \epsilon$, where $0 < \epsilon \ll 1$. Let m be the discrete state of an ideal diode. Then, the diode's static characteristic can be described as

$$mu_D - (1 - m)i_D = 0 \tag{82}$$

or

$$u_D = \underbrace{\frac{1-m}{m}}_{=:R(m)} i_D \tag{83}$$

For $m = \varepsilon$ (open switch), $R(m) = (1-\varepsilon)/\varepsilon$ takes a high value; for $m = 1-\varepsilon$ (open switch), $R(m)$ is of small value. In DBGs, switches may be denoted by the non-standard symbol $Sw : m$ regardless whether they are ideal, or non-ideal.

Single fault scenario

In an off-line simulation of a fault scenario, the physical system is replaced by a model. As has been shown in the previous sections, for linear models with ideal switches, a unique DAE system with mode-dependent coefficients can be obtained from a DBG with *fixed* causalities. However, the closing of an ideal switch may directly connect two storage elements so that one of their two ODEs becomes an algebraic equation. Consequently, the index of the DAE system may change when the circuit switches into another mode of operation. The problem in practice is that some simulation software such as Dymola[21] or OpenModelica can perform symbolic index reduction once prior to simulation but are not prepared to do so during simulation. After a change of the system mode the simulation may just fail with a division by zero. This problem and some remedies have been considered by Borutzky.[22] To overcome the problem, one may, for instance, add an ON resistance to at least some of the ideal switches. The resulting set of equations, however, may be stiff. When mode transitions take place, the numerical solution may fail. Changing parameters controlling the numerical integration such as the relative, or absolute tolerance, or the integration step size may help to recover, but the resulting accuracy may not be sufficient. Another option is to perform an index reduction prior to simulation for those system modes in which some ODEs turn into algebraic equations due to the closing of some switches. Then, for each system mode, a set ODEs is used.

Dynamic behaviour

In the following, the simple example with an ideal switch connecting two capacitors (Figure 4) is simulated. Computation of the dynamic behaviour starts with an open switch ($m = 1$) that closes at time instant $t_2 = 2$ ms ($m = 0$) and reopens again at $t_4 = 4$ ms

$$m(t) = 1 - \mathtt{pulse}(t, t_2, t_4) \tag{84}$$

For the time interval, in which the switch is closed, the DAE system has been reduced to an ODE system by differentiating the trivial algebraic equation $u_{C_1} = u_{C_2}$ prior to simulation. The fault scenario assumes that at time instant $t_3 = 1$ ms, capacitance C_1 abruptly reduces to half of its initial value

Table 2. Parameters of the circuit in Figure 4.

Parameter	Value	Units	Meaning
F	5.0	mA	Current source
R_1, R_2, R_3	1.0	kΩ	Resistances
C_1, C_2	1.0	μF	Capacitances
t_2	2.0	ms	Switch closes
t_4	4.0	ms	Switch reopens
t_3	1.0	ms	Capacitance C_1 drops to half of its value

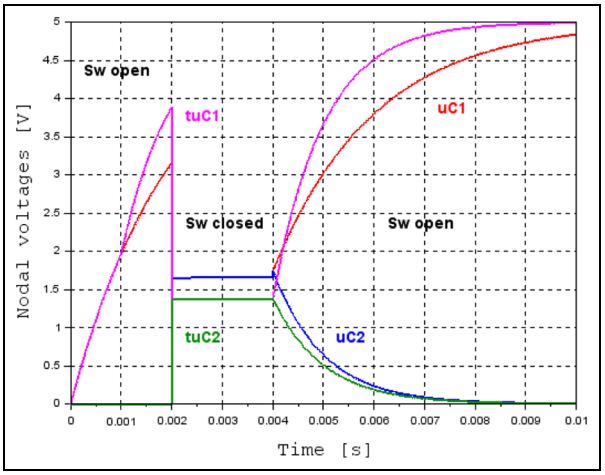

Figure 9. Time evolutions of the voltages u_{C_1}, u_{C_2} and of the voltages $\tilde{u}_{C_1}, \tilde{u}_{C_2}$ of the faulty circuit.

$$\tilde{C}_1(t) = C_1(1 - \mathtt{step}(t, t_3)) + \frac{C_1}{2}\mathtt{step}(t, t_3) \tag{85}$$

($\mathtt{step}(t, t_3)$ is the unit step function. The jump happens at $t = t_3$.)

Table 2 gives the parameters used in the simulation. Figure 9 shows the nodal voltages u_{C_1}, u_{C_2} of the faultless circuit as well as the faulty nodal voltages $\tilde{u}_{C_1}, \tilde{u}_{C_2}$ versus time. The latter ones are denoted as tuC_1 and tuC_2 in the figure. Simulation results have been obtained my means of the open software Scilab.[23]

As can be seen from Figure 9, the capacitor voltages discontinuously drop to a joint value at closing time $t_2 = 2ms$ of the ideal switch. This joint value, needed for a re-initialisation of the numerical integration, can be obtained from the principle of charge conservation. When the switch opens again, no re-initialisation is necessary as the time evolution of the two state variables continues with no jump.

In the faultless circuit, the closing switch causes an increase in the capacitance from C_1 to $C_1 + C_2 = 2C_1$ and a jump of both nodal voltages to the joint value of 1.58V. In the faulty circuit, capacitance C_1 reduces to half of its value at $t_3 = 1$ ms before the switch closes. As a result, the total capacitance at closing time is $(C_1/2 + C_2)$ and the joint value of both faulty capacitor voltages becomes

$$\tilde{u}_{C_1}(t_2^+) = \frac{\frac{C_1}{2}}{\left(\frac{C_1}{2} + C_2\right)} \tilde{u}_{C_1}(t_2^-) = 1.294\text{V} \tag{86}$$

where $\tilde{u}_{C_1}(t_2^-)$ denotes the left-side value of $\tilde{u}_{C_1}(t)$ at t_2 and $\tilde{u}_{C_1}(t_2^+)$ the right-side limit. Both joint voltage values 1.58V and 1.294V are in accordance with Figure 9. Due to the decrease in C_1 as of $t_3 < t_2$, the time constant for the loading of capacitor $\mathrm{C} : C_1$ becomes smaller. This is expressed by the increased rise of $\tilde{u}_{C_1}(t)$ in the interval $[t_3, t_2)$ and at t_4 when the switch disconnects the two circuit parts. Capacitor C_1 is charged with a time constant that is half of the time constant $\tau = (R_1 + R_2)C_1$ in the time interval $[0, t_3)$. For $0 < t < t_2$, the left part of the circuit is disconnected from the right one. Thus, the ODE for $\tilde{u}_{C_1}$ reads

$$\dot{\tilde{u}}_{C_1} + \frac{1}{(R_1 + R_2)\tilde{C}} \tilde{u}_{C_1} = \frac{R_1}{(R_1 + R_2)\tilde{C}} F \tag{87}$$

Hence

$$\dot{\tilde{u}}_{C_1}(t_3^-) = \frac{1}{(R_1 + R_2)\tilde{C}} \left(R_1 F - u_{C_1}(t_3^-)\right) \tag{88}$$

$$\dot{\tilde{u}}_{C_1}(t_3^+) = \frac{1}{(R_1 + R_2)\tilde{C}} \left(R_1 F - u_{C_1}(t_3^+)\right) \tag{89}$$

As a result

$$\dot{\tilde{u}}_{C_1}(t_3^+) = 2\dot{\tilde{u}}_{C_1}(t_3^-) = 3.0325 \times 10^{+3}\ \text{V/s} \tag{90}$$

In case the drop of capacitance C_1 takes place when the switch is closed, then this fault does not significantly affect the time evolution of u_{C_1} as long as the switch remains closed

$$\dot{\tilde{u}}_{C_1}(t_3^+) = \frac{4}{3} \dot{\tilde{u}}_{C_1}(t_3^-) \tag{91}$$

for $t_3 = (t_4 - t_2)/2$.

For $t > t_4$, capacitor C_2 is no longer connected to the current source and discharges with the time constant $R_3 C_2$.

Residuals

Let variables of the faulty system model carry a tilde. For instance, i_2^m becomes $\tilde{i}_2$. Residual r_1 then reads

$$\begin{aligned} r_1 &= -u_{\text{sw}} + R_1 F - R\tilde{i}_2 - \tilde{u}_{C_2} \\ &= -\frac{1}{\dot{q}_1} + R_1 F - R\tilde{i}_2 \\ &= -u_{C_1} + R_1 F - R\tilde{i}_2 \\ &= -u_{C_1} + R_1 F - R[\tilde{C}_1(t)\dot{\tilde{u}}_{C_1} + \tilde{i}_{\text{sw}}] \end{aligned} \tag{92}$$

In case the switch is open, $\tilde{i}_{\text{sw}} = 0$; otherwise, $\tilde{i}_{sw} = C_2\dot{\tilde{u}}_{C_2} + \tilde{u}_{C_2}/R_3$. Hence

$$\begin{aligned} r_1(t) = &-u_{C_1} + R_1 F \\ &- R\left[\tilde{C}_1(t)\dot{\tilde{u}}_{C_1} + \bar{m}(t)\left(C_2\dot{\tilde{u}}_{C_2} + \frac{1}{R_3}\tilde{u}_{C_2}\right)\right] \end{aligned} \tag{93}$$

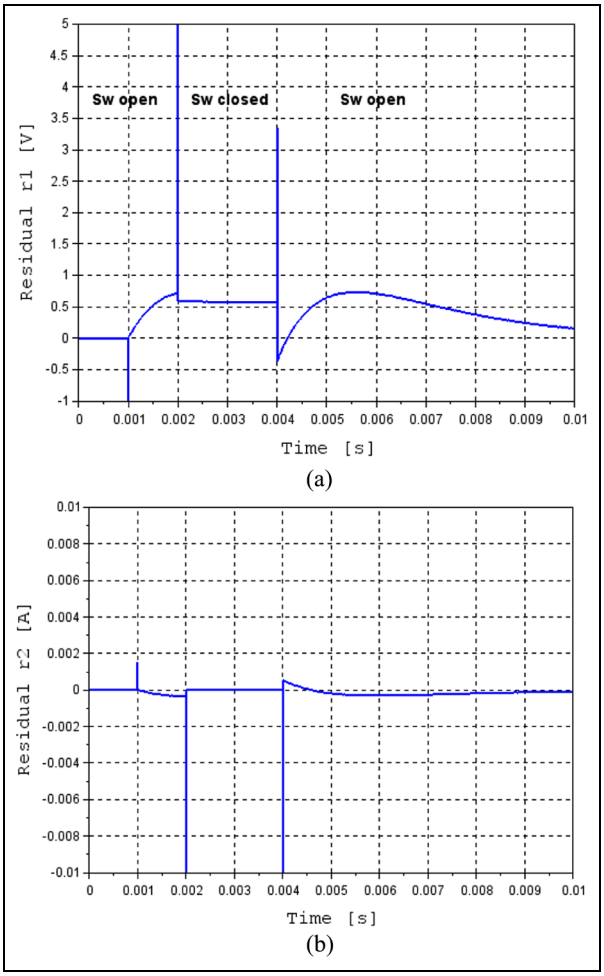

Figure 10. Residuals r_1, r_2 due to a drop of the capacitance C_1 at $t = 1$ ms: (a) residual r_1 and (b) residual r_2.

accounts for both cases. If the real circuit is not faulty, then $\tilde{C}_1 = C_1$ and $\tilde{u}_{C_1} = u_{C_1}, \tilde{u}_{C_2} = u_{C_2}$. As a result, $r_1 = 0$. In the same way, residual r_2 can be reformulated

$$\begin{aligned} r_2(t) = &-C_1\dot{u}_{C_1} - C_2\dot{u}_{C_2} - \tilde{i}_2 - \frac{1}{R_3}\tilde{u}_{C_2} \\ = &-C_1\dot{u}_{C_1} - C_2\dot{u}_{C_2} \\ &+ [\tilde{C}_1(t)\dot{\tilde{u}}_{C_1} + \bar{m}(t)(C_2\dot{\tilde{u}}_{C_2} + \tilde{u}_{C_2}/R_3)] \\ &- \frac{1}{R_3}\tilde{u}_{C_2} \end{aligned} \tag{94}$$

Figure 10(a) and (b) displays the response of residuals r_1, r_2 to an abrupt fault in capacitance C_1. Equation (94) indicates that residual r_2 depends on C_1 as expressed in the FSM. Figure 10(b), however, shows that r_2 is insensitive to changes in C_1. In fact, for both modes of operation, it can be proven analytically that $r_2(t) = 0$, for $0 \leqslant t \leqslant 0.01$ s.

Figure 10(a) shows that the response of residual r_1 to the abrupt fault of capacitance C_1 is mode-dependent. It captures the abrupt fault of parameter C_1 at $t_3 = 0.001$ s and decreases to zero when $u_{C_1}(t)$ approaches its final value $u_{C_1}(t \to \infty) = R_1 F = 5$ V independent of the value of C_1.

Conclusion

It has been shown that ARRs used in model-based FDI as well as a unique implicit state equation with mode-dependent coefficients can be obtained in a systematic manner from a *fixed*-causality DBG of a hybrid model in which switching components are represented by *ideal* switches.

Although ideal switches are naturally of variable causality, *fixed* causalities are assigned once to a DBG by means of the Sequential Causality Assignment Procedure (SCAP). Nevertheless, a unique set of equations is deduced from the DBG that determines the wanted residuals for all modes of operation. The key step is to substitute the JS outputs into the field of switches in the *implicit* switch equation.

The vector of residuals is a JS structure output into the field of detectors with inverted causalities. After some elimination steps, the residuals finally depend on the time derivative of the states and the switch outputs. For both unknowns an implicit DAE with mode-dependent. coefficients can be obtained.

For the DC motor drive example with two pairwise commutating switches, it has been shown that only a set of implicit algebraic equations is to be solved. Pairwise commutating switches can be identified by a causal path between their ports in a DBG.

For a faultless model with ideal switches, a unique implicit state equations with mode-dependent coefficients can be obtained from the ARRs.

The presented general matrix-based approach has been applied to three small illustrative example systems. Equations are directly deduced from a DBG and are reformulated so that they conform with the matrix equations obtained by the formal approach, based on a partitioning of the BG junction structure. For large-scale linear system models, the procedure can be implemented in a script or a programming language. For one of the three examples considered, a fault scenario has been simulated.

It has been outlined that the presented approach of using a fixed-causality DBG can also be applied in case some of the switches are to be considered non-ideal. The steps of the procedure do not need to be changed. A small change of the implicit equation of some switches, which actually turns it into an explicit one, is sufficient. Non-ideal switches, however, may result in a set of stiff equations, numerical problems, and a continuous approximation of discontinuous jumps.

The approach can be extended to mode-switching LTI models with uncertain parameters. The uncertain element parts can be collected into a field of sources modulated by power variables that is added to the block diagram in Figure 1. As a result, residuals depend on another additive term accounting for parameter uncertainties. Subject of further research may be an extension of the proposed approach to mode-switching system models with some non-linear elements.

Acknowledgements

This article is the result of a complete revision and a substantial extension of a paper entitled 'Generation of Mode-dependent ARRs from a Bond Graph of a Mode Switching LTI Model' presented at the 4th International Conference on Control, Decision and Information Technologies (CoDIT 2017), 5–7 April, 2017, Universitat Politècnica de Catalunya, Barcelona, Spain, USB Conference Proceedings.

Declaration of conflicting interests

The author(s) declared no potential conflicts of interest with respect to the research, authorship, and/or publication of this article.

Funding

The author(s) received no financial support for the research, authorship, and/or publication of this article.

References

1. Strömberg J, Top J and Södermann U. Variable causality in bond graphs caused by discrete effects. In: *International conference on bond graph modeling* (ed J Granda and F Cellier) *(ICBGM'93)*, La Jolla, CA, 17–20 January 1993, simulation series, vol. 25, no. 2, pp.115–119. Lyon: SCS Publishing.
2. Asher G. The robust modelling of variable topology circuits using bond graphs. In: *International conference on bond graph modeling* (ICBGM'93) (ed J Granda and F Cellier), La Jolla, CA, 17–20 January 1993, simulation series, vol. 25, no. 2, pp.126–131. Lyon: SCS Publishing.
3. Buisson J, Cormerais H and Richard PY. Analysis of the bond graph model of hybrid physical systems with ideal switches. *Proc IMECHE, Part I: J Systems and Control Engineering* 2002; 216(1): 47–63.
4. Margetts R. *Modelling & analysis of hybrid dynamic systems using a bond graph approach*. PhD thesis, University of Bath, Bath, 2013.
5. Mosterman P. *Hybrid dynamic systems: a hybrid bond graph modeling paradigm and its application in diagnosis*. PhD thesis, Vanderbilt University, Nashville, TN, 1997.
6. Samantaray A and Ould Bouamama B. *Model-based process supervision: a bond graph approach (advances in industrial control)*. London: Springer, 2008.
7. Samantaray A, Medjaher K, Ould Bouamama B, et al. Diagnostic bond graphs for online fault detection and isolation. *Simul Model Pract Th* 2006; 14(3): 237–262.
8. Medjaher K and Zerhouni N. Residual-based failure prognostic in dynamic systems. IFAC Proceedings Volumes, Vol. 42, Issue 8, pp. 716 – 721 https://doi.org/10.3182/20090630-4-ES-2003.00119 https://www.sciencedirect.com/science/article/pii/S1474667016358621
9. Borutzky W (ed.). *Bond graphs for modelling, control and fault diagnosis of engineering systems*. 2nd ed. Cham: Springer, 2016.
10. Borutzky W. *Bond graph model-based fault diagnosis of hybrid systems*. Cham: Springer, 2015.
11. Wang D, Yu M, Low C, et al. *Model-based health monitoring of hybrid systems*. New York: Springer, 2013.

12. Borutzky W. Bond-graph-based fault detection and isolation for hybrid system models. *Proc IMechE, Part I: J Systems and Control Engineering* 2012; 226(6): 742–760.
13. Ducreux J, Dauphin-Tanguy G and Rombaut C. Bond graph modelling of commutation phenomena in power electronic circuits. In: *International conference on bond graph modeling (ICBGM'93)* (ed J Granda and F Cellier), La Jolla, CA, 17–20 January 1993, simulation series, vol. 25, no. 2, pp.132–136. Lyon: SCS Publishing.
14. Ould Bouamama B, Samantaray A and Staroswiecki M, et al. Derivation of constraint relations from bond graph models for fault detection and isolation. In: *International conference on bond graph modeling (ICBGM'03)* (ed J Granda and F Cellier), Orlando, FL, 19–23 January 2003, simulation series, vol. 35, no. 2, pp. 104–109. Lyon: SCS Publishing.
15. HighTec Consultants. Symbols Shakti™ (reference manual), 2006 https://www.researchgate.net/publication/257351148Users_Manual_of_SYMBOLS_Shakti.
16. Ould Bouamama B, Samantaray AK, Medjaher K, et al. Model builder using functional and bond graph tools for FDI design. *Control Eng Pract* 2005; 13(7): 875–891.
17. Merzouki R, Samantaray A, Pathak P, et al. *Intelligent mechatronic systems*. Berlin: Springer, 2013.
18. Touati Y, Merzouki R and Ould Bouamama B. Fault detection and isolation in presence of input and output uncertainties using bond graph approach. In: *5th international conference on integrated modeling and analysis in applied control and automation (IMAACA)* (ed A Bruzzone, G Dauphin-Tanguy, S Junco, et al.), Rome, 12–14 September 2011, pp.21–227. Genoa: University of Genoa.
19. Rosenberg R. State-space formulation for bond graph models of multiport systems. *J Dyn Syst: T ASME* 1971; 93(1): 35–40.
20. Mosterman P and Biswas G. A theory of discontinuities in physical system models. *J Franklin Inst* 1998; 335(3): 401–439.
21. Dassault Systèmes, 2015, http://www. Dymola.com
22. Borutzky W. A new approach to the derivation of a single set of implicit state equations from a fixed causality bond graph of a hybrid model. In: *10th international conference on integrated modelling and analysis in applied control and automation (IMAACA)* (ed A Bruzzone, G Dauphin-Tanguy, S Junco, et al.), Barcelona, 18–20 September 2017. USB conference proceededings, pp 9 – 16, DIME, Universitá di Genoa, Italy.
23. Scilab Enterprises. Scilab, Versailles, https://www.scilab.org/